batteries

MDPI

Article

Organic Rankine Cycle as the Waste Heat Recovery Unit of Solid Oxide Fuel Cell: A Novel System Design for the Electric Vehicle Charging Stations Using Batteries as a Backup/Storage Unit

Hossein Pourrahmani *, Chengzhang Xu and Jan Van herle

Group of Energy Materials, École Polytechnique Fédérale de Lausanne, 1951 Sion, Switzerland
* Correspondence: hossein.pourrahmani@epfl.ch

Abstract: The novelty of this study is to suggest a novel design for electric vehicle charging stations using fuel cell technology. The proposed system benefits from the Organic Rankine Cycle (ORC) to utilize the exhaust energy of the Solid Oxide Fuel Cell (SOFC) stacks in addition to the Lithium-Ion battery to improve the efficiency by partial-load operation of the stacks at night. The study is supported by the thermodynamic analysis to obtain the characteristics of the system in each state point. To analyze the operation of the system during the partial-load operation, the dynamic performance of the system was developed during the day. Furthermore, the environmental impacts of the system were evaluated considering eighteen parameters using a life-cycle assessment (LCA). LCA results also revealed the effects of different fuels and working fluids for the SOFC stacks and ORC, respectively. Results show that the combination of SOFC and ORC units can generate 264.02 kWh with the respective overall energy and exergy efficiencies of 48.96% and 48.51%. The suggested 264.02 kWh contributes to global warming (kg CO_2 eq) by 5.17×10^5, 8.36×10^4, 2.5×10^5, 1.98×10^5, and 6.79×10^4 using methane, bio-methanol, natural gas, biogas, and hydrogen as the fuel of the SOFC stacks.

Keywords: electric vehicle charging station; thermodynamic analysis; life-cycle assessment; dynamic performance; solid oxide fuel cell (SOFC)

Citation: Pourrahmani, H.; Xu, C.; Van herle, J. Organic Rankine Cycle as the Waste Heat Recovery Unit of Solid Oxide Fuel Cell: A Novel System Design for the Electric Vehicle Charging Stations Using Batteries as a Backup/Storage Unit. *Batteries* **2022**, *8*, 138. https://doi.org/10.3390/batteries8100138

Academic Editor: Palani Balaya

Received: 26 July 2022
Accepted: 20 September 2022
Published: 22 September 2022

1. Introduction

The limited fossil fuel resources and their harmful impacts on the environment have been the main motivations for researchers to find alternative solutions [1]. At the moment, the prime mover for most vehicles and power plants is based on combustion engines that use fossil fuels [2]. Renewable energies such as wind and solar are recently being widely used for power plants and buildings, while hydrogen and methane have shown promising results to be used for mobile applications [3]. These two fuels can be either directly injected into modified combustion engines or be used in fuel cells, which utilize electrochemical reactions to generate electricity [4]. The usage of fuel cells in power plants and charging stations ensures a continuous and environmentally friendly generation of electricity for different types of applications [5].

The most commercialized types of fuel cells are the Solid Oxide Fuel Cell (SOFC) [6] and Proton Exchange Membrane Fuel Cell (PEMFC) [7], which operate in high- and low-temperatures, respectively. PEMFC only uses hydrogen as the fuel [8], while SOFC can utilize methane, methanol, bio-methanol, natural gas, and biogas in addition to hydrogen [9]. SOFC is considered to be more suitable for stationary applications such as power plants and charging stations, either standalone [10] or combined with other renewable resources such as wind [11], solar [12], and geothermal [13]. As the operating temperature of the SOFC is high, the exhaust gases from the stack may still have the energy to be

recovered [14]. In this regard, it is common to integrate the SOFC units with different types of bottoming cycles [15]. The selection of the bottoming cycle mainly depends on the temperature of the output flow from the afterburner of the SOFC unit. In high-temperature cases, the usage of gas turbines is suggested [16], while the Kalina cycle and Organic Rankine Cycle (ORC) have shown promising results in low exhaust temperatures [17]. The waste heat recovery of the SOFC unit also leads to higher efficiencies of the system while improving the environmental performance of the SOFC units by reducing the waste heat to the atmosphere.

Thus far, the usage of ORCs has been recognized in more than 690 power plants with more than 2.6 Gigawatts of installed capacity [18]. The most important application of the ORCs is to recover the waste heat by different types of units, in addition to being used in biomass, solar, wind-thermal, and geothermal power plants [19]. In the operation of the ORCs, the selection of the working fluid is of importance and the efficiency of the system is highly dependent on the thermodynamic characteristics of the utilized working fluid [20]. The ideal properties for the ORC's working fluids are isentropic vapor saturation curve, low freezing point, safety, low cost, and low environmental impacts [21]. Although there have been studies to indicate the better performance of the combined systems from energetic and exergetic aspects, there is a research gap on the environmental impacts of using the integrated systems of the SOFC and ORC.

Instead of characterizing the environmental impacts of the SOFC's operation, a detailed analysis should be deployed to consider all the processes to manufacture the SOFC and all the other components of the hybrid system in addition to the processes needed for the SOFC's operation, i.e., maintenance [22]. In this regard, a comprehensive study should be conducted to evaluate the supply chain of the components and their life cycles, which is known as a life-cycle assessment (LCA) [23]. Using LCA, all the environmental effects of the combined system are obtained during the entire lifetime from the extraction of the raw materials to the manufacturing of the components of the integrated system and the disposal of waste and emissions to the environment at each stage of the life cycle [24]. This study aims to suggest an integrated system to provide electricity for a charging station for electric vehicles using fuel cell technology that is environmentally friendly. However, the processes of the whole operation of the charging station should be further analyzed using the LCA method to make a logical comparison to the conventional fossil-fuel-based systems.

Furthermore, as a method to reduce the possible harmful impacts on the environment and improve the efficiency of the integrated system, the usage of batteries is suggested [25]. Therefore, partial operation of the system becomes feasible, which means lower disposal of heat to the environment and a higher lifetime of the system. In this condition, the efficiency of the system will be improved as well [26]. Although there has been implementation of different types of storage systems in an integrated system to improve the overall performance, a detailed dynamic evaluation [27] of the combined battery in the proposed system should be performed in addition to the energy, exergy, and environmental studies to prove the suitability of the system to be established as a charging station for the electric cars.

Due to the harmful impacts of fossil fuels on the environment, the main aim of this study is to propose an integrated system using the four SOFC stacks as the energy provider. The system is designed to provide the required electricity for a charging station that is dedicated to electric vehicles. To better improve the efficiency of the system, the exhaust heat of the SOFC stacks is recovered by an ORC unit considering R134a as the working fluid. As the power demand of the electric cars may vary during the day, it is assumed that the four SOFC stacks will operate full-load (100%) during the day from 6 a.m. to 10 p.m., while three of the SOFC stacks will change to partial-load (30%) operation from 10 p.m. to 6 a.m. to reduce waste to the environment and to improve the efficiency of the combined system. The fourth SOFC stack will remain at full-load operation. Since there is still a possibility of having fluctuations in the power demand by the electric cars, a $LiMn_2O_4$ type of Lithium-Ion battery is integrated to the SOFC stacks, and the ORC unit is to be charged during the full-load operation and act as a backup system for the possible lack of electricity

during the partial operation of the SOFC stacks. A dynamic study of the battery considering three different power demands was performed to better analyze the performance of the dedicated battery in the system. Energy and exergy characterizations were performed to obtain the thermodynamic properties in all the state points and to calculate the overall efficiencies and exergy destructions. Additionally, the LCA method was used to figure out the impacts of the current suggested design on the environment. Comparisons were also made between the environmental impacts of different input fuels for the SOFC stacks and ORC's working fluids.

2. Problem Description

At the current stage, there are power plants, which are fueled by fossil fuels to produce power for different applications. However, this study aims to find a suitable alternative for fossil-fueled power plants to act as a charging station for electric vehicles. In this regard, four SOFC stacks are devised to use methane as the fuel and produce the main share of the required electricity. To operate the SOFC, the fuel, air, and water are compressed to reach the desired pressure followed by pre-heating to obtain the required temperature. Then, the steam and the fuel are mixed in a mixer before entering the SOFC stack. During the operation of the SOFC, electricity is generated that is transferred to the inverter, and the exhaust gases are transported to the afterburner. The reason behind using the afterburner is the existence of gases which have not participated in the electrochemical reactions and still have enough chemical energy to be converted. After the combustion in the afterburner, the exhaust gases from this unit have a noticeable amount of heat to be recovered by a bottoming cycle. The temperature of the exhaust streams from the SOFC stacks remains higher than 1000 K after passing through the water and fuel pump heat exchanger, however, the exhaust temperature decreases rapidly through the air pump heat exchanger to temperature below 500 K. The mass flow is large and stays constant during the heat exchange process. To recover the exhaust heat of the SOFC stacks, ORC with R134a as the working fluid is utilized to further generate electricity for the proposed charging station. It should be mentioned that a basic ORC unit is used for heat recovery purposes, and advanced ORC units such as cascaded ORC and ORC with regenerator will obviously further recover the exhaust heat from the SOFC stacks. Figure 1 shows a schematic of the proposed design to provide electricity for electric vehicles. In Figure 1, WP, FC, AC, WPH, FPH, APH, AF, ORC, and SOFC are the respective abbreviations for the water pump, fuel compressor, water pre-heater, fuel pre-heater, air pre-heater, afterburner, Organic Rankine Cycle, and Solid Oxide Fuel Cell.

To improve the efficiency of the system and reduce the amount of required fuel for the system's operation, the SOFC stacks operate full-load (100%) during the day from 6 a.m. to 10 p.m. while SOFC1, SOFC2, and SOFC3 work partial-load (30%) from 10 p.m. to 6 a.m. considering that SOFC4 continues full-load operation. The reason behind this strategy is that there are fewer electric cars at night requiring to be charged, hence, it is better to decrease the system's operation and fuel utilization. However, it is possible that a sudden peak in the power demand occurs, either during the day or at night. In this regard, it is suggested to use batteries to store the electricity once the power demand is lower than the generated electricity by the SOFC stacks and the ORC unit, hence, the battery can act as a backup unit in high power demand scenarios.

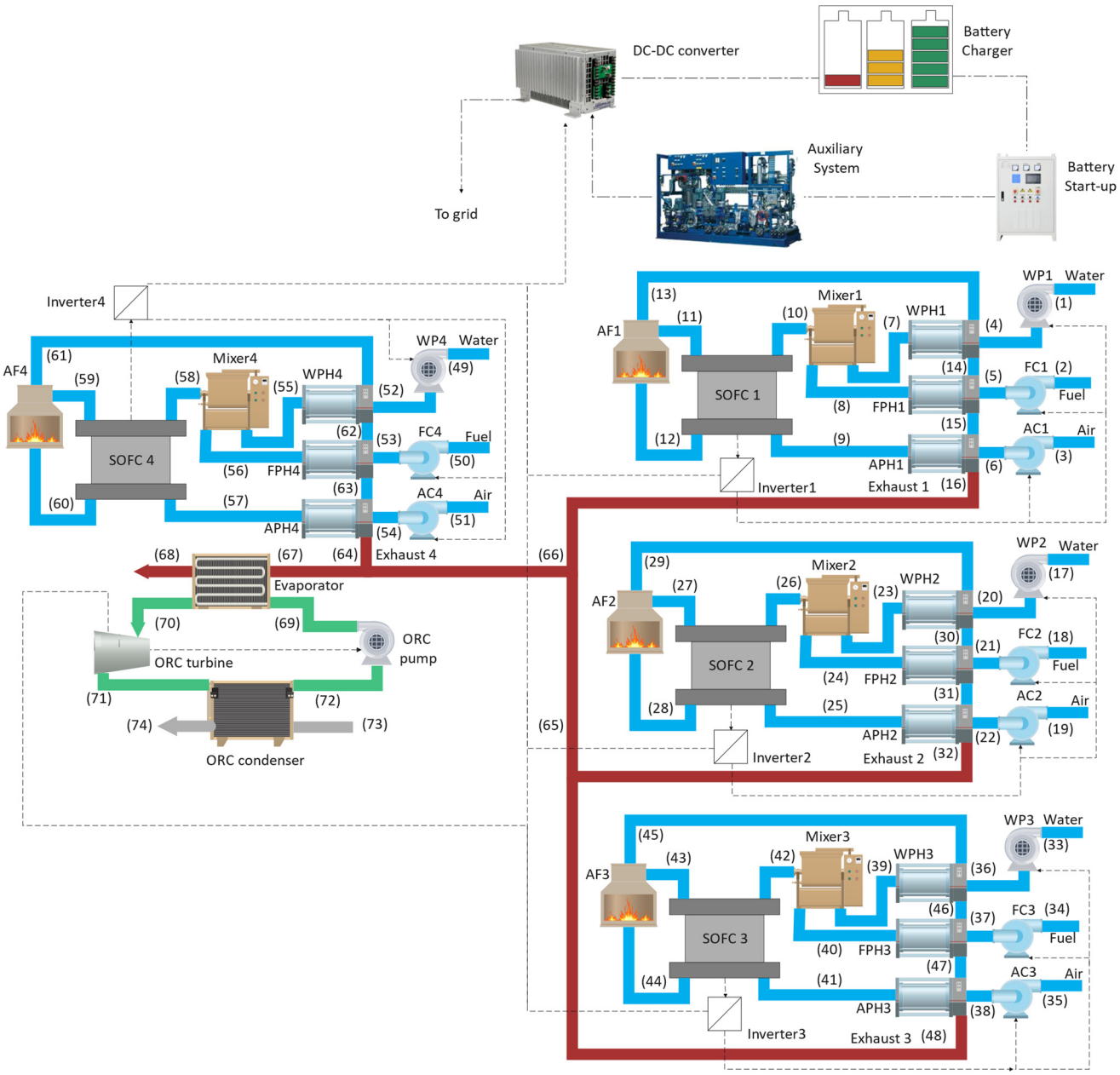

Figure 1. The suggested system design that uses ORC and SOFC units to generate the required electricity for the charging station benefiting from the batteries as the backup/storage.

In addition to a dynamic performance needed to analyze the response of the battery to different power load demands, the performance of the system should be characterized by a detailed thermodynamic analysis to obtain the energetic and exergetic characteristics in addition to the overall efficiencies. Although the usage of methane and fuel cells seems to be more environmentally friendly than fossil fuels, a detailed life-cycle assessment is still needed to figure out the corresponding impacts of this charging station considering eighteen parameters based on ReCiPe 2016 v1.03 Midpoint (H).

3. Thermodynamic Modeling

In the first step, the thermodynamic analysis of the SOFC stacks and ORC unit of the integrated system given in Figure 1 are developed to obtain the overall output power of the charging station. In this regard, a thermodynamic model is needed, which also enables the calculation of the overall efficiencies. It is noteworthy to mention that the utilized battery,

which acts as a backup/storage unit, is not included in the thermodynamic model, and a separate dynamic analysis is used to characterize the performance of the battery. To obtain the thermodynamic properties of each state point in the integrated design given in Figure 1, the modeling was developed in MATLAB software. Once the thermodynamic analysis and dynamic response of the system are performed, a comprehensive LCA study evaluates the impacts of the system on the environment considering different SOFC fuels and ORC working fluids.

3.1. Solid Oxide Fuel Cell (SOFC)

The operations of the SOFC stacks are dependent on the chemical reactions that occur in an SOFC [28]. At first, the methane reacts with steam water to produce hydrogen as follows:

$$CH_4 + H_2O \rightarrow 3H_2 + CO \tag{1}$$

Then, the hydrogen reacts with the existing oxygen in the air to generate electricity and water:

$$H_2 + \frac{1}{2}O_2 \rightarrow H_2O + e^- \tag{2}$$

If the output current from this electrochemical reaction is being considered as i (A/cm^2), the output power from the SOFC can be calculated as follows:

$$W_{SOFC} = iA_{cell}N_{cell}V_{cell} \tag{3}$$

where A_{cell} (cm^2) is the active surface area, N_{cell} is the number of cells, and V_{cell} (V) is the cell's voltage, which is shown in Equation (4):

$$V_{cell} = V_N - V_{act} - V_{ohm} - V_{conc} \tag{4}$$

The subscripts N, act, ohm, and conc refer to the Nernst, activation, ohmic, and concentration voltages, respectively. Additionally, Equation (5) represents the Nernst voltage:

$$V_N = \left(-\frac{\Delta g_s}{nF}\right) - \frac{R_u T_{cell}}{nF} \ln\left(\frac{P_{H_2O}}{P_{H_2}\sqrt{P_{O_2}}}\right) \tag{5}$$

where F (C/mol) is the Faraday's constant, R_u (m^3 Pa K^{-1} mol^{-1}) is the universal gas constant, T_{cell} (K) is the cell's operating temperature, Δ_{g_s} (kJ/kmol) is the variation in the Gibbs free energy, n is the transported electrons in a reaction, and P_i (bar) is the partial pressure dedicated for each gas. Equations (6) and (7) demonstrate the energy and exergy efficiencies for the SOFC stacks:

$$\eta_{en} = \frac{\dot{W}_{net}}{\dot{m}_{fuel}LHV_{fuel}} \tag{6}$$

$$\eta_{ex} = \frac{\dot{W}_{net}}{\dot{m}_{fuel}ex_{fuel}} \tag{7}$$

where $\dot{W}_{net}$ (kW/s) is the net generated power by SOFC, $\dot{m}$ (mol/s) is the mass flow rate, LHV (kJ/kmol) is the low heating value, and ex_{fuel} (kJ/kmol) is the chemical exergy of the fuel.

3.2. Organic Rankine Cycle (ORC)

Considering the R134a as the working fluid, the saturation condition can be reached in the evaporator as follows:

$$\dot{Q}_{in,ORC} = \dot{m}_{67}(h_{68} - h_{67}) = \dot{m}_{69}(h_{70} - h_{69}) \quad (8)$$

where $\dot{Q}_{in,ORC}$ (W/s) is the exhaust heat by the four SOFC stacks. Equation (9) shows the needed relation to predict the generated power in the ORC's turbine:

$$\dot{W}_{ORC,turbine} = \dot{m}_{70}(h_{70} - h_{71}) \quad (9)$$

With a similar approach, Equation (10) demonstrates the required power by the ORC's pump:

$$\dot{W}_{ORC,pump} = \dot{m}_{72}(h_{69} - h_{72}) \quad (10)$$

Equations (11) and (12) also present the corresponding values for the energy and exergy efficiencies:

$$\eta_{en} = \frac{\dot{W}_{ORC,turbine} - \dot{W}_{ORC,pump}}{\dot{Q}_{in,ORC}} \quad (11)$$

$$\eta_{ex} = \frac{\dot{W}_{ORC,turbine} - \dot{W}_{ORC,pump}}{\dot{E}x_{in,ORC}} \quad (12)$$

3.3. Exergy Analysis

To calculate the exergy values in each thermodynamic state, the chemical and physical exergies should be summed. As an assumption, it should be noted that the physical exergy values are equal to zero at the inlet flow of the units, which enables the calculation of the exergy values in each state point of the integrated system using the exergy balance equations presented in Table 1. Once the exergy values in each thermodynamic state given in Figure 1 are obtained, the prediction of the overall exergy efficiency and the exergy destructions in each component become feasible. Equations (13) and (14) present the corresponding formulas to calculate the overall energy and exergy efficiencies of the proposed charging station.

$$\eta_{energy} = \frac{\dot{W}_{net,\ SOFC,\ 1,2,3,4} + \dot{W}_{net,\ ORC}}{\dot{Q}_{net,in}} \quad (13)$$

$$\eta_{exergy} = \frac{\dot{W}_{net,\ SOFC,\ 1,2,3,4} + \dot{W}_{net,\ ORC}}{\dot{m}_{fuel} ex_{fuel}} \quad (14)$$

where $\dot{Q}_{net}$ in Equation (13) is the given energy by the input fuel to the SOFC stacks and can be calculated as follows:

$$\dot{Q}_{net,in} = \dot{m}_{fuel} LHV_{fuel} \quad (15)$$

Table 1. Exergy balance equations for the current integrated system.

Component	Exergy Balance Equation
SOFC 1	
SOFC stack	$\dot{E}x_{10}^{ch} + \dot{E}x_{10}^{ph} + \dot{E}x_{9}^{ch} + \dot{E}x_{9}^{ph} = \dot{E}x_{11}^{ch} + \dot{E}x_{11}^{ph} + \dot{E}x_{12}^{ch} + \dot{E}x_{12}^{ph} + \dot{E}x_{D,\,SOFC}$
Water pump	$\dot{E}x_1 + W_{WP} = \dot{E}x_4 + \dot{E}x_{D,WP}$
Fuel compressor	$\dot{E}x_2 + W_{comp} = \dot{E}x_5 + \dot{E}x_{D,comp}$
Air compressor	$\dot{E}x_3 + W_{comp} = \dot{E}x_6 + \dot{E}x_{D,comp}$
Water pre-heater	$\dot{E}x_{13} + \dot{E}x_4 = \dot{E}x_7 + \dot{E}x_{14} + \dot{E}x_{D,WPH}$
Fuel pre-heater	$\dot{E}x_{14} + \dot{E}x_5 = \dot{E}x_8 + \dot{E}x_{15} + \dot{E}x_{D,FPH}$
Air pre-heater	$\dot{E}x_{15} + \dot{E}x_6 = \dot{E}x_9 + \dot{E}x_{16} + \dot{E}x_{D,APH}$
Fuel mixer	$\dot{E}x_7 + \dot{E}x_8 = \dot{E}x_{10} + \dot{E}x_{D,mixer}$
Afterburner	$\dot{E}x_{11} + \dot{E}x_{12} = \dot{E}x_{13} + \dot{E}x_{D,afterburner}$
Exhausts of SOFC	
Mix 1	$\dot{E}x_{16} + \dot{E}x_{65} = \dot{E}x_{66} + \dot{E}x_{D,mix\ 1}$
Mix 2	$\dot{E}x_{48} + \dot{E}x_{32} = \dot{E}x_{65} + \dot{E}x_{D,mix\ 2}$
Mix 3	$\dot{E}x_{66} + \dot{E}x_{64} = \dot{E}x_{67} + \dot{E}x_{D,mix\ 3}$
ORC	
Evaporator	$\dot{E}x_{67} + \dot{E}x_{69} = \dot{E}x_{68} + \dot{E}x_{70} + \dot{E}x_{D,evap}$
Turbine	$\dot{E}x_{70} = \dot{E}x_{71} + W_{turbine} + \dot{E}x_{D,turbine}$
Condenser	$\dot{E}x_{71} + \dot{E}x_{73} = \dot{E}x_{72} + \dot{E}x_{74} + \dot{E}x_{D,condenser}$
Pump	$\dot{E}x_{69} + W_{pump} = \dot{E}x_{72} + \dot{E}x_{D,pump}$

4. Results and Discussion

4.1. Thermodynamic Analysis

Once the thermodynamic model of the SOFC stacks and ORC unit were developed in the MATLAB software, the REFPROP 9.0 [29] library was used to perform the simulation and calculate the thermodynamic properties. Table 2 shows the needed parameters to evaluate the thermodynamic properties in each state point of the charging station given in Figure 1. It should be noted that the operation of the SOFC has been previously validated by the current authors in Reference [30], and the results are not given here to prevent repetition.

Table 2. Input operating parameters to perform the energy and exergy analyses.

Parameters	Value
SOFC	
Inlet temperature	1000 K
Number of cells	600
Operating pressure	1.013 bar
Operating temperature	298.15 K
Pressure drop in the afterburner	0.03
Pressure drop in the heat exchanger	0.02
Pressure drop in the SOFC	0.02
Pressure ratio of compressor	1.19
Steam to carbon ratio	2.5
Surface area	100 cm^2
ORC	
Pump isentropic efficiency	0.85
Turbine isentropic efficiency	0.85

Using the input parameters given in Table 2, the thermodynamic simulation can be performed and the thermodynamic properties can be obtained in each state point of the system, which is shown in Figure 1. Table 3 presents the thermodynamic properties of the SOFC stacks including the temperature, pressure, mass flow rates, entropy, etc., while

Table 4 shows the similar output characteristic of the ORC unit in the respective state points from 69 to 74, shown in Figure 1. It should be noted that the evaporating temperature at the ORC unit is estimated using the pinch point temperature difference considering the pressure ratio of the pump and condensation temperature. The obtained thermodynamic properties by Tables 3 and 4 enable the calculation of the overall energy efficiency of the system based on Equation (13) in addition to predicting the exergy values using exergy balance equations in Table 1. Once the exergy values are obtained, the exergy destruction in each component and the overall exergy efficiency, given by Equation (14), can be calculated. Table 5 shows the corresponding values of the overall energy and exergy efficiency in addition to the total output power of the system to be used in the charging station and the required mass flow rate of fuel as the input. It is noteworthy to mention that Table 3 also presents the characteristics of the temperature and mass flow rate of exhaust energy in SOFC1, SOFC2, SOFC3, and SOFC4 by the given properties in states 16, 32, 48, and 64, respectively.

Table 3. The thermodynamic properties of the state variables of the SOFC stacks at 0.7 A/cm^2.

State	T (K)	P (bar)	$\dot{m}$ ($\frac{mol}{s}$)	s ($\frac{kJ}{kg \cdot K}$)	ex (kW)	Mole Fraction Percentage			
						H_2O	H_2	O_2	N_2
1	298.15	1.01	0.52	6.62	0	100	0	0	0
2	298.15	1.01	0.21	186.22	0	0	0	0	0
3	298.15	1.01	15.71	6.86	0	0	0	21	79
4	298.15	1.20	0.52	6.62	0	100	0	0	0
5	314.83	1.20	0.21	186.88	0.09	0	0	0	0
6	316.02	1.20	15.71	6.86	1374	0	0	21	79
7	1000	1.17	0.52	168.14	11.43	100	0	0	0
8	1000	1.17	0.21	246.78	4.21	0	0	0	0
9	1000	1.17	15.71	234.40	175.56	0	0	21	79
10	1000	1.17	0.73	240.83	189.16	71.43	0	0	0
11	1077	1.16	1.32	240.73	63.23	71.26	10.56	0	0
12	1077	1.16	17.56	236.68	198.74	0	0	19.24	80.76
13	1135	1.12	16.44	241.43	3.68	5.73	0	17.53	75.43
14	1079	1.10	16.44	239.79	213.31	5.73	0	17.53	75.43
15	1066.5	1.08	16.44	239.54	207.49	5.73	0	17.53	75.43
16	441.5	1.06	16.44	211.77	13238	5.73	0	17.53	75.43
17	298.15	1.01	0.52	6.62	0	100	0	0	0
18	298.15	1.01	0.21	186.22	0	0	0	0	0
19	298.15	1.01	15.71	6.86	0	0	0	21	79
20	298.15	1.20	0.52	6.62	0	100	0	0	0
21	314.84	1.20	0.21	186.88	0.09	0	0	0	0
22	316.02	1.20	15.71	6.86	1374	0	0	21	79
23	1000	1.17	0.52	168.14	11.43	100	0	0	0
24	1000	1.17	0.21	246.78	4.21	0	0	0	0
25	1000	1.17	15.71	234.40	175.56	0	0	21	79
26	1000	1.17	0.73	240.83	189.16	71.43	0	0	0
27	1077	1.16	1.32	240.73	63.23	71.26	10.56	0	0
28	1077	1.16	17.56	236.68	198.74	0	0	19.24	80.76
29	1135	1.12	16.44	241.43	3.68	5.73	0	17.53	75.43
30	1079	1.10	16.44	239.79	213.31	5.73	0	17.53	75.43
31	1066.5	1.08	16.44	239.54	207.49	5.73	0	17.53	75.43
32	441.5	1.06	16.44	211.77	13238	5.73	0	17.53	75.43
33	298.15	1.01	0.52	6.61	0	100	0	0	0
34	298.15	1.01	0.21	186.22	0	0	0	0	0
35	298.15	1.01	15.71	6.86	0	0	0	21	79

Table 3. *Cont.*

State	T (K)	P (bar)	$\dot{m}$ ($\frac{mol}{s}$)	s ($\frac{kJ}{kg \cdot K}$)	ex (kW)	Mole Fraction Percentage			
						H_2O	H_2	O_2	N_2
36	298.15	1.20	0.52	6.61	0	100	0	0	0
37	314.84	1.20	0.21	186.88	0.09	0	0	0	0
38	316.02	1.20	15.71	6.86	1374	0	0	21	79
39	1000	1.17	0.52	168.14	11.43	100	0	0	0
40	1000	1.17	0.21	246.78	4.21	0	0	0	0
41	1000	1.17	15.71	234.40	175.56	0	0	21	79
42	1000	1.17	0.73	240.83	189.16	71.43	0	0	0
43	1077	1.16	1.32	240.73	63.23	71.26	10.56	0	0
44	1077	1.16	17.56	236.68	198.74	0	0	19.24	80.76
45	1135	1.12	16.44	241.43	3.68	5.73	0	17.53	75.43
46	1079	1.10	16.44	239.79	213.31	5.73	0	17.53	75.43
47	1066.5	1.08	16.44	239.54	207.49	5.73	0	17.53	75.43
48	441.5	1.06	16.44	211.77	13238	5.73	0	17.53	75.43
49	298.15	1.01	0.52	6.62	0	100	0	0	0
50	298.15	1.01	0.21	186.22	0	0	0	0	0
51	298.15	1.01	15.71	6.86	0	0	0	21	79
52	298.15	1.20	0.52	6.61	0	100	0	0	0
53	314.84	1.20	0.21	186.88	0.09	0	0	0	0
54	316.02	1.20	15.71	6.86	1374	0	0	21	79
55	1000	1.17	0.52	168.14	11.43	100	0	0	0
56	1000	1.17	0.21	246.78	4.21	0	0	0	0
57	1000	1.17	15.71	234.40	175.56	0	0	21	79
58	1000	1.17	0.73	240.83	189.16	71.43	0	0	0
59	1077	1.16	1.32	240.73	63.23	71.26	10.56	0	0
60	1077	1.16	17.56	236.68	198.74	0	0	19.24	80.76
61	1135	1.12	16.44	241.43	3.68	5.73	0	17.53	75.43
62	1079	1.10	16.44	239.79	213.31	5.73	0	17.53	75.43
63	1066.5	1.078	16.44	239.54	207.49	5.73	0	17.53	75.43
64	441.5	1.057	16.44	211.77	13238	5.73	0	17.53	75.43
65	441.5	1.057	32.89	211.77	13238	5.73	0	17.53	75.43
66	441.5	1.057	49.33	211.77	13238	5.73	0	17.53	75.43
67	441.5	1.057	65.78	211.77	13238	5.73	0	17.53	75.43
68	301	1.036	65.78	199.78	3295	5.73	0	17.53	75.43

Table 4. The thermodynamic properties of the state variables in the ORC.

State	T (K)	P (bar)	$\dot{m}$ ($\frac{mol}{s}$)	s ($\frac{kJ}{kg \cdot K}$)	ex (kW)
69	299.8725	33.269	13.0588	1.1212	59.9039
70	372	33.269	13.0588	1.718	99.6331
71	303.3802	6.6538	13.0588	1.734	57.0369
72	298.15	6.6538	13.0588	1.1199	56.9755
73	298.15	1.013	1689.0515	6.8586	60433
74	303.15	1.013	1689.0515	6.8754	60433

Table 5. The corresponding system performance results at the current density of 7.0 (A/cm^2).

Parameter	Value
Fuel consumption	3.35 g/s
Total output power	246.02 kW
Overall energy efficiency	48.96%
Overall exergy efficiency	48.51%

By the calculation of the exergy values using Tables 1, 3, and 4, the prediction of the exergy destructions in each component of the system becomes feasible. In this regard,

important information about the efficiencies and the irreversibilities of each component of the system are obtained, which enables improved monitoring of the system. Figure 2 shows the corresponding figure of the exergy destructions in each component of the system. As it can be seen, the air pre-heaters of the SOFC stacks have by far the highest exergy destruction values followed by the afterburners, where the combustion of the unreacted exhaust gases from the SOFC stack occurs. The results of Figure 2 also clearly indicate the low exergy destruction values in the related components to the ORC unit in comparison to the SOFC stacks.

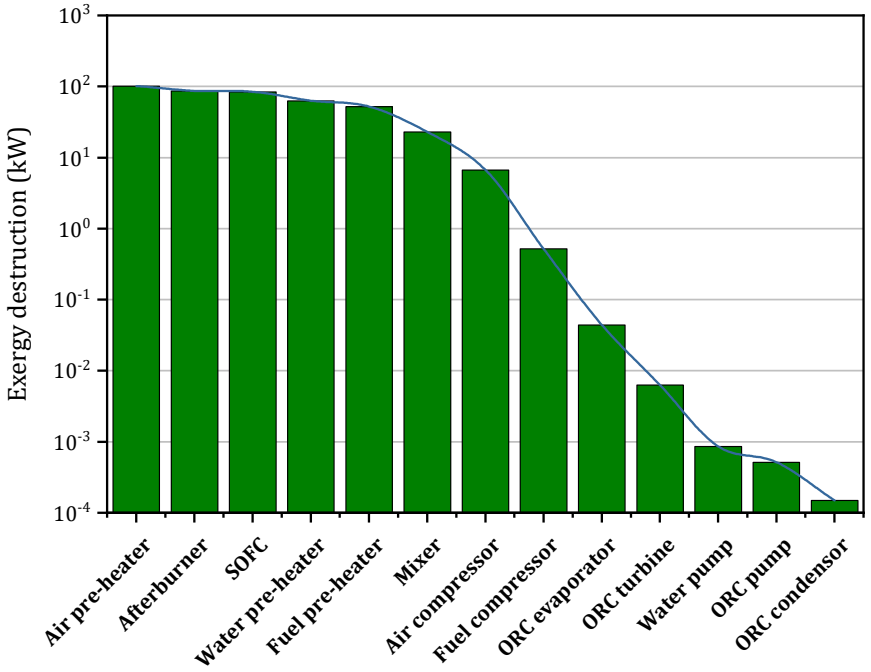

Figure 2. Exergy destruction of the utilized components in the integrated design.

An important parameter in the performance of the suggested design of the charging station, given in Figure 1 using the SOFC technology, is the operating current density. Although performing the sensitivity analysis to understand the effective parameters on the system performance is valuable in most of the multi-generation systems, the results of the sensitivity analysis can be predicted due to the importance of the SOFC current density, fuel utilization, and fuel on the output performance. The variation in the SOFC's current density leads to considerable changes in the output power and the exhaust heat by the SOFC stacks. Therefore, as the exhaust values of the SOFC stacks change by the variation in the current density, the corresponding output power of the ORC unit is subjected to the changes by the variation in the SOFC's current density. Figure 3 illustrates the respective values of the output power by the SOFC stacks and the ORC unit at seven different current densities. As a function of the output powers of the SOFC stacks and ORC unit, the overall energy and exergy efficiencies will change by the variation in the SOFC's current density. Figure 4 demonstrates the corresponding changes in the overall efficiencies by the changes in the SOFC's current density. As it can be seen, although higher current densities result in higher output powers from the SOFC stacks and ORC unit, lower overall efficiencies are being observed in high current densities. The reasons for this phenomenon based on Equations (13) and (14) is the higher intake of heat and higher exergy values in the case of overall energy and exergy efficiencies, respectively.

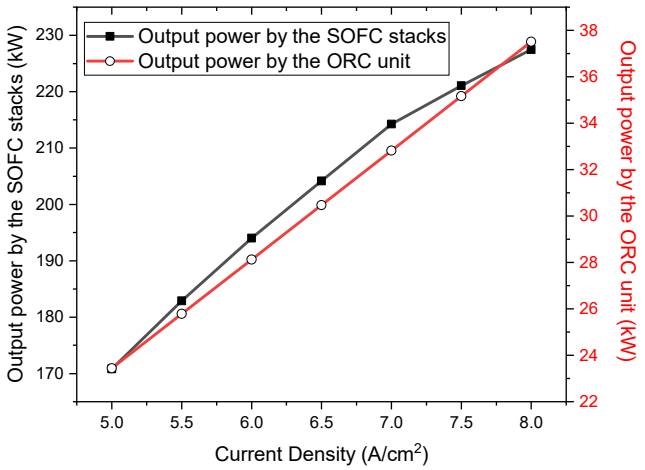

Figure 3. The changes in the output powers of the SOFC stacks and the ORC unit by the variation in the SOFC's current density.

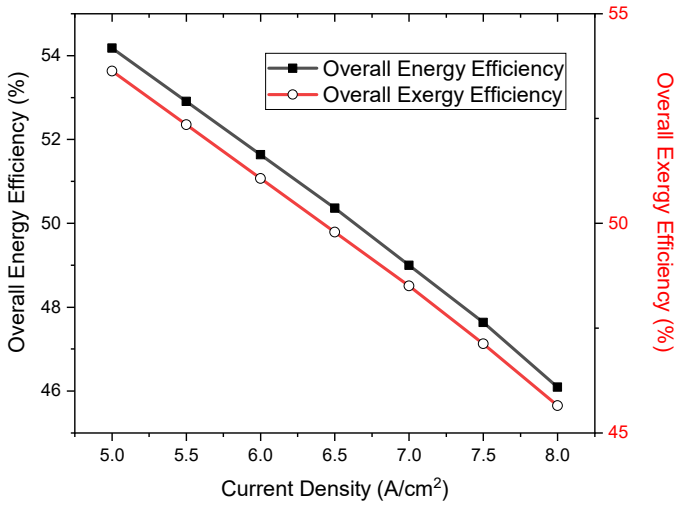

Figure 4. The changes in the overall efficiencies by the variation in the SOFC's current density.

4.2. Dynamic Response

As mentioned in Section 2, the aim of using the battery in the integrated design of the charging station is to reduce the operation time and fuel utilization of the SOFC stacks. In other words, based on Figure 1, SOFC4 operates full-load during the day, while SOFC1, SOFC2, and SOFC3 operate full-load from 6 a.m. to 10 p.m. followed by a part-load operation (30%) from 10 p.m. to 6 a.m., hence lowering the degradation and improving the lifetime of the SOFC stacks. Table 6 presents the required input parameters to analyze the performance of the battery in the given condition of the charging station.

Table 6. The required input parameters of the battery to perform the dynamic analysis.

Parameters	Value
Voltage across cell	2.1 (V)
Maximum discharge rate	C/5
Maximum charge rate	C/10
Maximum cell capacity	50 (A h)
Lower capacity limit of battery	20%
Maximum capacity limit of battery	100%
Efficiency of charge controller	98%

The goal of using the battery is to store the surplus generated electricity by the SOFC stacks and ORC unit when the power demand by the electric vehicle is low. Then, the battery can act as a backup unit once the power demand is higher than the output produced power by the SOFC and ORC units. To evaluate the response of the battery to the changes in the power demand, three different power load demands were selected based on the given patterns by Gilleran et al. [31] with some modifications to match the output power of the current system. Figure 5 illustrates the three different power load profiles that are considered to characterize the dynamic response of the battery.

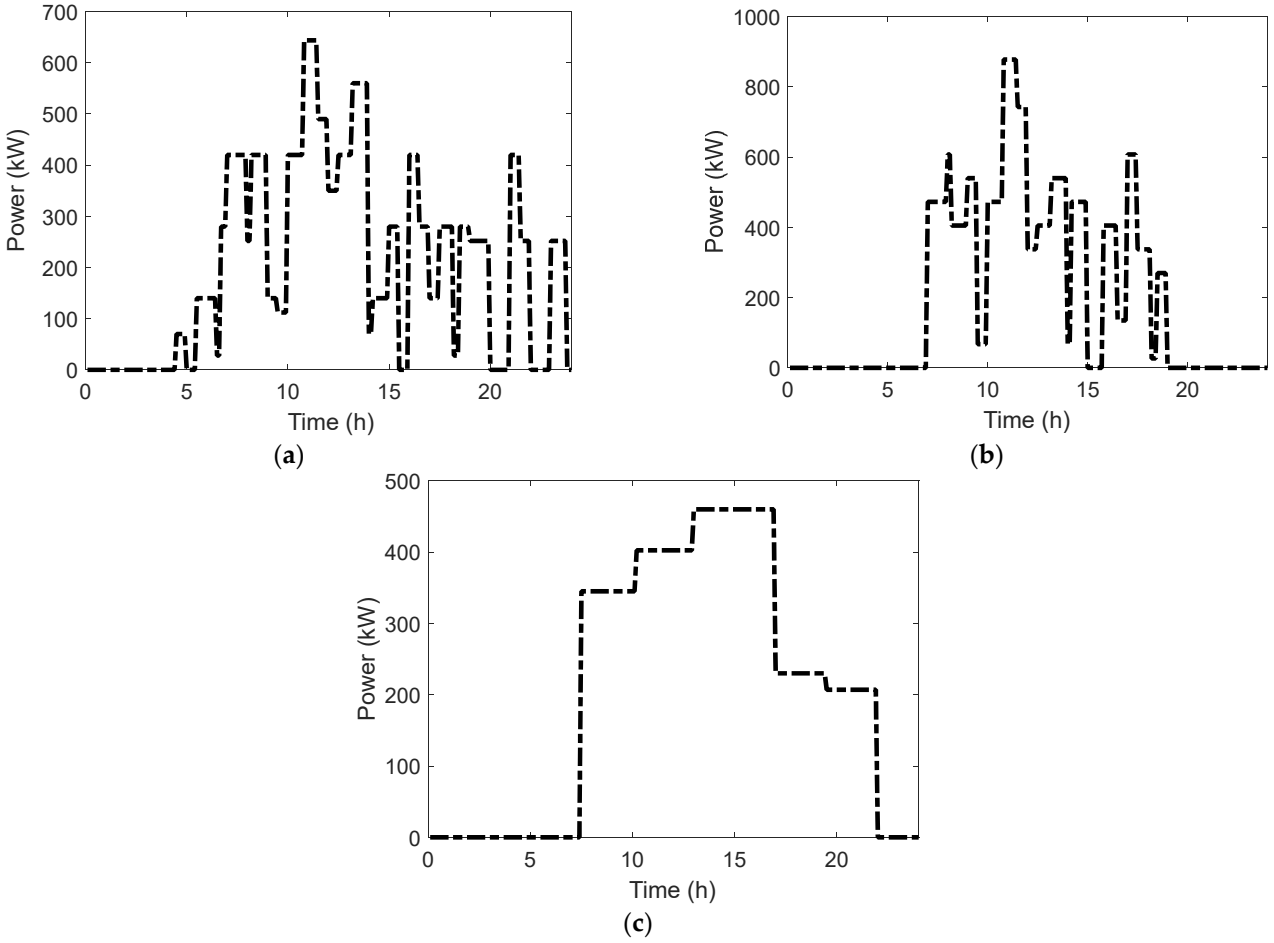

Figure 5. Three different power demand profiles of the proposed system: (**a**) first power load profile, (**b**) second power load profile, and (**c**) third power load profile.

The results of the dynamic responses of the utilized battery in the integrated design of the charging station considering the three different power load profiles of Figure 5 are shown in Figure 6. As it can be seen, the system is capable enough to store the required electricity and act as a backup unit in the case of a sudden peak in the power demand during the day. Figure 6 also shows that the charging of the battery is mainly conducted during the night once the power demand is low, and discharging occurs during daylight.

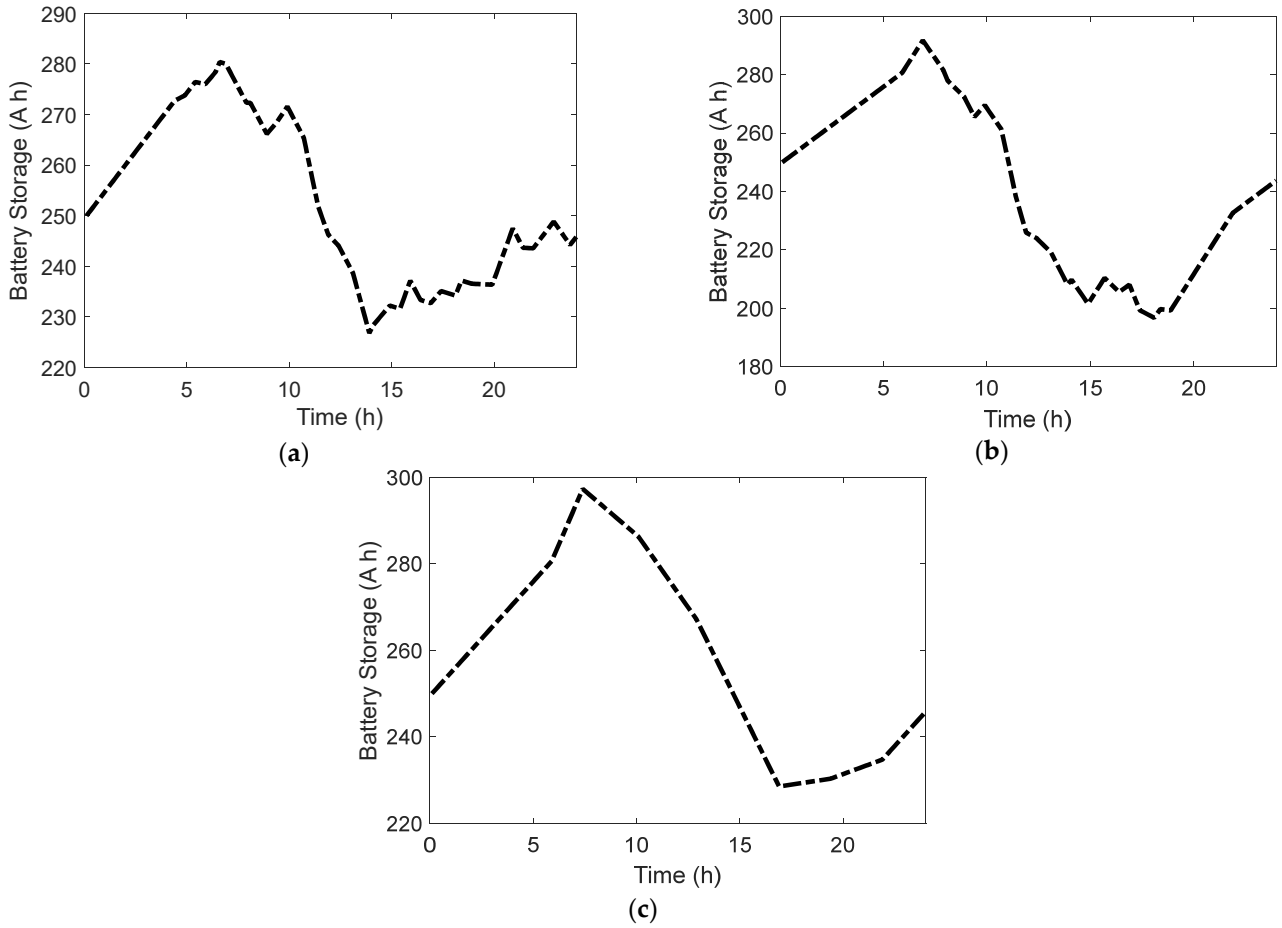

Figure 6. The changes in the storage of battery in different power demand profiles of the proposed system: (**a**) first power load profile, (**b**) second power load profile, (**c**) third power load profile.

4.3. Life-Cycle Assessment (LCA)

As mentioned in Section 1, LCA is a technique to obtain the environmental impacts of the whole operation of the proposed system from the extraction of the raw materials to the production of electricity by the SOFC and ORC units. The selected LCA methodology frameworks are the ISO 14040 and 14044 [32,33], using the ReCiPe 2016 v1.03 Midpoint (H) method [34] with the openLCA software, which is an open-source software to perform LCA. Additionally, the ecoinvent database [35], which benefits from a transparent unit-process LCI database, was used to obtain the required information for the selected materials and operations. Table 7 presents the needed materials, equipment, facilities, and transportations that are required to construct and operate the proposed charging station of the electric vehicles using SOFC, ORC, and battery units.

Table 7. The required material inputs to perform LCA analysis considering methanol as the SOFC's fuel and R134a as ORC's working fluid [36–38].

Inputs	Values
Air	1638 kg
Alumina	10 kg
Aluminum oxide sealer	84 kg
Anode graphite for Li-Ion battery	250 kg

Table 7. *Cont.*

Inputs	Values
Battery separator	250 kg
Cerium Lanthanum Yttrium Carbonate Phosphor	29.4 kg
Chlorine	163.2 kg
Dibutylphthalate	2.88 kg
Ethanol	44.88 kg
Ethylene Glycol Polyol	2.88 kg
Heat by the onsite boiler	44.28 GJ
Heating and sanitary equipment	0.48 items
Inverter	40 items
Iron–Nickel–Chromium alloy	40 kg
Lanthanum oxide	270.24 kg
Li-Ion battery cell	250 kg
$LiMn_2O_4$ cathode for Li-Ion battery	250 kg
Medium voltage electricity	1.07 MWh
Methane	48.24 kg
Nickel	0.024 kg
Nickel, 99.5%	4 kg
Nickel, Ni 2.5E+0%, in mixed ore	18.72 kg
Nitric acid, without water, in 50% solution state	1367.04 kg
ORC for heat and power co-generation	1 unit
Petroleum coke	26.88 kg
Polyvinyl butyral (PVB)	7.44 kg
Sheet rolling, chromium steel	328 kg
Sheet rolling, steel	1880 kg
SOFC maintenance	4 units
SOFC stacks	4 units
Spray drying process	57 GJ
Steel reinforcement bare; blast furnace route	1880 kg
Steel, chromium steel 18/8	488 kg
Transport freight, sea, container ship	2.0544×10^4 t.km
Transport, freight train	3756.8 t.km
Transport, freight, light commercial vehicle	100 t.km
Transport, freight, lorry 16–32 metric ton, EURO6	512 t.km
Transport, lorry >28 t, fleet average—US	256 t.km
Transport, lorry 16–32 t, EURO3—US	576 t.km
Urea, as N	672 kg
Water	135.72 kg
Water for manufacturing	12.48 m^3
Water, deionized	236.16 kg
Zirconium Chloride powder	199.68 kg
Zirconium oxide	18.72 kg

Having in mind the mentioned methodology and database to perform the LCA, the corresponding impacts of the suggested design of the charging station using the SOFC, ORC, and battery units are analyzed considering eighteen different parameters. Table 8 presents the eighteen different impact categories based on ReCiPe 2016 v1.03 Midpoint (H) for the designed 246.02 kWh charging station illustrated in Figure 1. The results are also compatible with the performed analyses by Strazza et al. [37], Ding et al. [36], and [38], which were dedicated to the LCA studies of SOFC, ORC, and the $LiMn_2O_4$ Lithium-Ion battery.

Table 8. The obtained LCA results of the ReCiPe 2016 v1.03 Midpoint (H) impact categories for the suggested design of the 246.02 kWh charging station.

Impact Category	Unit	Impact Result
Fine particulate matter formation	kg PM2.5-eq	1.65×10^3
Fossil resource scarcity	kg oil-eq	1.33×10^5
Freshwater ecotoxicity	kg 1,4-DCB eq	1.49×10^5
Freshwater eutrophication	kg P-eq	3.37×10^2
Global warming	kg CO_2 eq	5.17×10^5
Human carcinogenic toxicity	kg 1,4-DCB eq	1.42×10^5
Human non-carcinogenic toxicity	kg 1,4-DCB eq	1.58×10^6
Ionizing radiation	kBq Co-60-eq	2.93×10^4
Land use	m^2a crop-eq	1.35×10^4
Marine ecotoxicity	kg 1,4-DCB eq	1.91×10^5
Marine eutrophication	kg N-eq	1.86×10^1
Mineral resource scarcity	kg Cu eq	1.86×10^4
Ozone formation, human health	kg NO_x eq	1.48×10^3
Ozone formation, terrestrial ecosystems	kg NO_x-eq	1.54×10^3
Stratospheric ozone depletion	kg CFC11-eq	1.04
Terrestrial acidification	kg SO_2-eq	3.76×10^3
Terrestrial ecotoxicity	kg 1,4-DCB eq	7.71×10^6
Water consumption	m^3	4.71×10^3

Additionally, the given LCA methodology and the eighteen impact categories, which were mentioned in Table 8, are characterized by five main input categories, namely, (1) manufacturing, (2) mining, extraction, and supply, (3) maintenance, (4) transport and distribution, and (5) disposal. Figure 7 illustrates the shares of the five input categories on the environment during the operation of the 246.02 kWh charging station. As it can be seen, manufacturing has by far the largest share of global warming, human carcinogenic toxicity, water consumption, terrestrial acidification/ecotoxicity/ecosystems, land use, freshwater eutrophication, and mineral resource scarcity. Figure 7 also indicates that the disposal has the main shares in marine ecotoxicity/eutrophication, stratospheric ozone depletion, human non-carcinogenic toxicity, fossil resource scarcity, fine particulate matter formation, and ionizing radiation. Furthermore, mining, extraction, and supply has the largest impact on freshwater ecotoxicity and ozone formation, human health.

It should be noted that the results of Table 8 and Figure 7 are obtained assuming methane as the SOFC's fuel and R134a as the ORC's working fluid. In this regard, analyzing different types of SOFC fuels and ORC working fluids and their respective impacts on the environment can be valuable to select the optimum working conditions. Table 9 considers five different types of SOFC fuel, namely, methane, bio-methanol, natural gas, biogas, and hydrogen, and presents a detailed comparison of their impacts on the environment. As it can be seen, hydrogen is the most environmentally friendly fuel for the SOFC's stacks in many of the impact categories, while other types of fuels such as methane, biogas, and bio-methanol are promising candidates when pure hydrogen is not available.

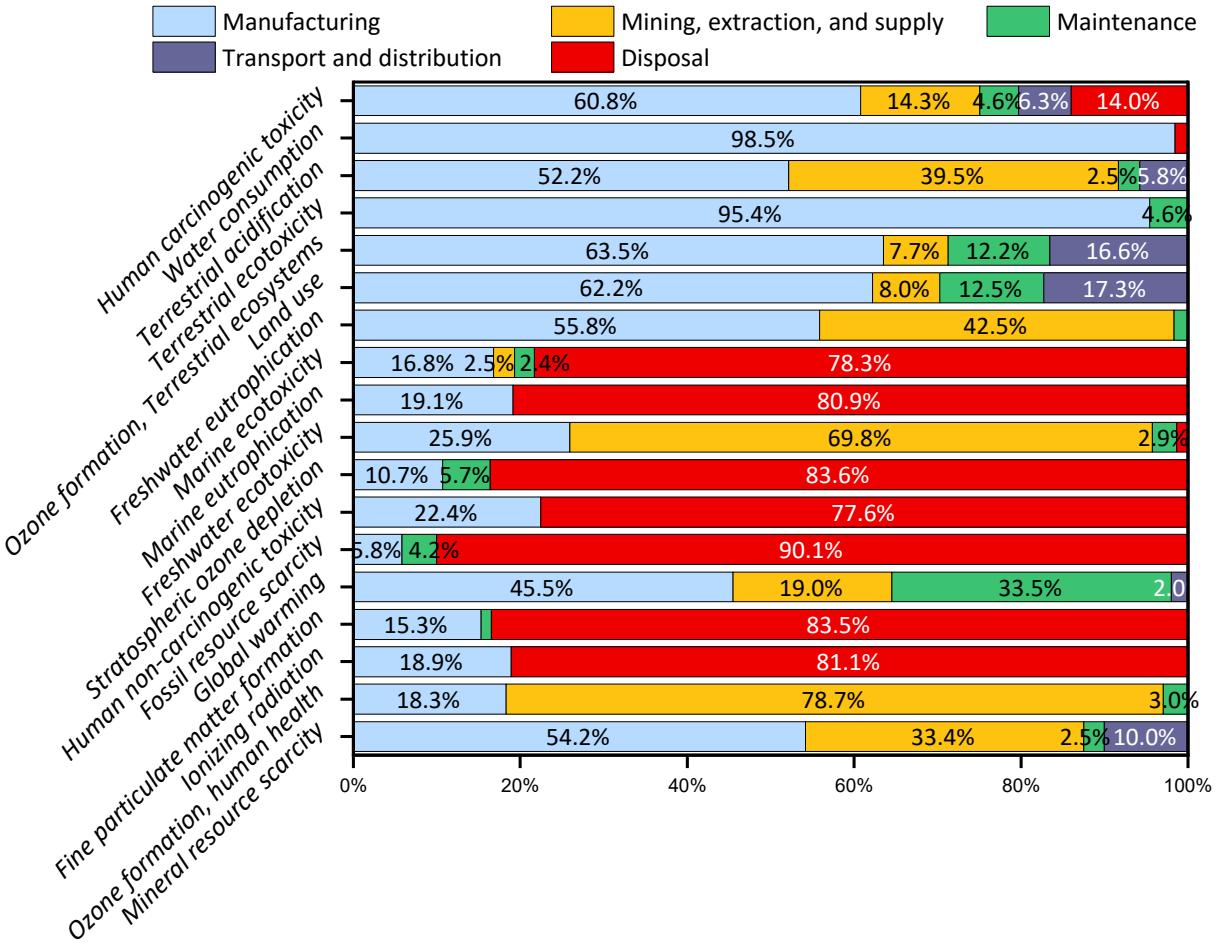

Figure 7. The shares of different procedures on the environment during the operation of the 246.02 kWh charging station.

Table 9. The comparison between different types of input fuel for the SOFC stacks and their impacts on the environment based on ReCiPe 2016 v1.03 Midpoint (H) for the suggested design of the 246.02 kWh charging station.

Impact Category	Unit	Methane	Bio-Methanol	Natural Gas	Biogas	Hydrogen
Fine particulate matter formation	kg PM2.5-eq	1.65×10^{3}	9.60×10^{3}	4.23×10^{2}	1.07×10^{3}	2.77×10^{2}
Fossil resource scarcity	kg oil-eq	1.33×10^{5}	2.84×10^{4}	6.84×10^{4}	1.46×10^{4}	3.84×10^{4}
Freshwater ecotoxicity	kg 1,4-DCB eq	1.49×10^{5}	3.18×10^{4}	7.66×10^{4}	1.64×10^{4}	4.30×10^{4}
Freshwater eutrophication	kg P-eq	3.37×10^{2}	5.48×10^{2}	6.65×10^{1}	5.34×10^{1}	7.60×10^{1}
Global warming	kg CO_2 eq	5.17×10^{5}	8.36×10^{4}	2.50×10^{5}	1.98×10^{5}	6.79×10^{4}
Human carcinogenic toxicity	kg 1,4-DCB eq	1.42×10^{5}	2.30×10^{4}	6.87×10^{4}	5.44×10^{4}	1.86×10^{4}
Human non-carcinogenic toxicity	kg 1,4-DCB eq	1.58×10^{6}	2.55×10^{5}	7.64×10^{5}	6.05×10^{5}	2.08×10^{5}
Ionizing radiation	kBq Co-60-eq	2.93×10^{4}	4.74×10^{3}	1.42×10^{4}	1.12×10^{4}	3.85×10^{3}
Land use	m^2a crop-eq	1.35×10^{4}	2.18×10^{3}	6.53×10^{3}	5.17×10^{3}	1.77×10^{3}
Marine ecotoxicity	kg 1,4-DCB eq	1.91×10^{5}	3.09×10^{4}	9.24×10^{4}	7.31×10^{4}	2.51×10^{4}
Marine eutrophication	kg N-eq	1.86×10^{1}	3.03×10^{1}	3.67	2.95	4.2
Mineral resource scarcity	kg Cu eq	1.86×10^{4}	3.03×10^{4}	3.67×10^{3}	2.95×10^{3}	4.20×10^{3}
Ozone formation, human health	kg NO_x eq	1.48×10^{3}	3.92×10^{2}	9.34×10^{2}	2.28×10^{2}	2.74×10^{2}
Ozone formation, terrestrial ecosystems	kg NO_x-eq	1.54×10^{3}	1.54×10^{3}	9.69×10^{2}	2.37×10^{2}	2.84×10^{2}
Stratospheric ozone depletion	kg CFC11-eq	1.04	2.76×10^{-1}	6.58×10^{-1}	1.61×10^{-1}	1.93×10^{-1}
Terrestrial acidification	kg SO_2-eq	3.76×10^{3}	9.94×10^{2}	2.37×10^{3}	5.80×10^{2}	6.95×10^{2}
Terrestrial ecotoxicity	kg 1,4-DCB eq	7.71×10^{6}	2.04×10^{6}	4.86×10^{6}	1.19×10^{6}	1.43×10^{6}
Water consumption	m^3	4.71×10^{3}	1.25×10^{3}	2.97×10^{3}	7.26×10^{2}	8.71×10^{2}

Moreover, Table 10 considers four different ORC working fluids, namely, R134a, R227ea, R152a, and R245fa, and makes a comparison between their impacts on the environment based on ReCiPe 2016 v1.03 Midpoint (H). The results show that R245fa is the most environmentally friendly working fluid for the ORC, followed by R152a and R134a. Table 10 also suggests against the usage of R227ea, considering the environmental aspects.

Table 10. The comparison between different types of ORC's working fluids and their impacts on the environment based on ReCiPe 2016 v1.03 Midpoint (H) for the suggested design of the 246.02 kWh charging station.

Impact Category	Unit	R134a	R227ea	R152a	R245fa
Fine particulate matter formation	kg PM2.5-eq	1.65×10^3	2.29×10^3	1.48×10^3	1.27×10^3
Fossil resource scarcity	kg oil-eq	1.33×10^5	1.84×10^5	1.20×10^5	1.02×10^5
Freshwater ecotoxicity	kg 1,4-DCB eq	1.49×10^5	2.06×10^5	1.34×10^5	1.15×10^5
Freshwater eutrophication	kg P-eq	3.37×10^2	4.67×10^2	3.03×10^2	2.59×10^2
Global warming	kg CO_2 eq	5.17×10^5	7.16×10^5	4.65×10^5	3.98×10^5
Human carcinogenic toxicity	kg 1,4-DCB eq	1.42×10^5	1.97×10^5	1.28×10^5	1.09×10^5
Human non-carcinogenic toxicity	kg 1,4-DCB eq	1.58×10^6	2.19×10^6	1.42×10^6	1.22×10^6
Ionizing radiation	kBq Co-60-eq	2.93×10^4	4.06×10^4	2.64×10^4	2.25×10^4
Land use	m^2a crop-eq	1.35×10^4	1.87×10^4	1.21×10^4	1.04×10^4
Marine ecotoxicity	kg 1,4-DCB eq	1.91×10^5	2.65×10^5	1.72×10^5	1.47×10^5
Marine eutrophication	kg N-eq	1.86×10^1	2.58×10^1	1.67×10^1	1.43×10^1
Mineral resource scarcity	kg Cu eq	1.86×10^4	2.58×10^4	1.67×10^4	1.43×10^4
Ozone formation, human health	kg NO_x eq	1.48×10^3	2.05×10^3	1.33×10^3	1.14×10^3
Ozone formation, terrestrial ecosystems	kg NO_x-eq	1.54×10^3	2.13×10^3	1.39×10^3	1.19×10^3
Stratospheric ozone depletion	kg CFC11-eq	1.04	1.44	9.36×10^{-1}	8.00×10^{-1}
Terrestrial acidification	kg SO_2-eq	3.76×10^3	5.21×10^3	3.38×10^3	2.89×10^3
Terrestrial ecotoxicity	kg 1,4-DCB eq	7.71×10^6	1.07×10^7	6.94×10^6	5.93×10^6
Water consumption	m^3	4.71×10^3	6.52×10^3	4.24×10^3	3.62×10^3

5. Conclusions

The current paper evaluated a state-of-the-art design for the electric vehicle charging station using SOFC, ORC, and battery units. Thermodynamic modeling and simulation were developed to obtain the characteristics of the system in each state point. Having these characteristics enabled the calculation of the output power, overall efficiencies, and exhaust heat. Results indicated that the system is able to produce 246.02 kWh electricity using 3.35 g/s of methane. The respective overall energy and exergy efficiencies were also calculated to be 48.96% and 48.51%. The changes in the current density of the SOFC stacks resulted in noticeable changes in the output power of the SOFC stacks and ORC unit, followed by changes in the overall efficiencies. Although higher current densities resulted in higher output powers, the efficiencies are reduced since the operation of SOFC stacks at high current densities leads to higher exergy values and exhaust heat. The results of the exergy destructions in each component also indicated the low exergy destruction values between the ORC's components, while the SOFC's air pre-heater had the highest share among all the analyzed components.

The dynamic response of the $LiMn_2O_4$ battery by three different power load profiles was analyzed, and it was concluded that the battery unit is capable enough to act as a backup/storage unit for the possible fluctuations in the power demand of the electric vehicles. Results of the life-cycle assessment also showed the impacts of the current suggested design of the charging station on the environment using the ReCiPe 2016 v1.03 Midpoint (H). A comparison was made to analyze the effects of five different SOFC fuels, which resulted in the conclusion of selecting pure hydrogen as the most environmentally friendly fuel for the SOFC. However, the LCA results also indicated the promising results of bio-methanol, biogas, and methane to be used as the SOFC's fuel once pure hydrogen is not available. The second comparison among the impacts of the different ORC's working fluid

on the environment revealed the advantages of using R245fa. The LCA results suggested against using R227ea based on the ReCiPe 2016 v1.03 Midpoint (H). Although the current study covered important gaps in the literature, the following topics can be interesting for future studies:

- The current study performed a detailed energy, exergy, and environmental study to characterize the overall performance of the suggested design for the charging station. In addition to this study, it is suggested to perform an economic evaluation to further characterize this novel design using thermo-economic or exergo-economic methodologies.
- This study considered the usage of a $LiMn_2O_4$ Lithium-Ion battery to act as the backup/storage unit. Although the $LiMn_2O_4$ battery has shown promising results in different applications, other types of batteries and storage systems can be further analyzed and integrated into the system. LCA studies can be conducted for each type of battery and the obtained simulation results can facilitate the determination of the best type of battery to be used in the suggested design.

Author Contributions: Methodology, H.P., Software—Life cycle assessment, H.P., Formal analysis, H.P., Visulaization, H.P., Writing—Original draft, H.P., Writing – Review and editing, H.P., Project administration, H.P., Software—thermodynamic analysis, C.X., Conceptualization, C.X., Supervision, J.V.h. All authors have read and agreed to the published version of the manuscript.

Funding: This project received funding from the European Union's Horizon 2020 Research and Innovation program under the Marie Sklodowska-Curie grant agreement no. 754354.

Data Availability Statement: The data is available upon formal request.

Conflicts of Interest: The authors declare no conflict of interest.

References

1. Pourrahmani, H.; Shakeri, H.; Van Herle, J. Thermoelectric generator as the waste heat recovery unit of proton exchange membrane fuel cell: A numerical study. *Energies* **2022**, *15*, 3018. [CrossRef]
2. Gharehghani, A.; Pourrahmani, H. Performance evaluation of diesel engines (PEDE) for a diesel-biodiesel fueled CI engine using nano-particles additive. *Energy Convers. Manag.* **2019**, *198*, 111921. [CrossRef]
3. Gay, M.; Pourrahmani, H.; Van Herle, J. Fuel cell and battery technologies for a 800 kW ferry: Two optimized scenarios. *Sci. Talks* **2022**, *3*, 100039. [CrossRef]
4. Pourrahmani, H.; Siavashi, M.; Yavarinasab, A.; Matian, M.; Chitgar, N.; Wang, L.; Van Herle, J. A review on the long-term performance of proton exchange membrane fuel cells: From degradation modeling to the effects of bipolar plates, sealings, and contaminants. *Energies* **2022**, *15*, 5081. [CrossRef]
5. Pourrahmani, H.; Gay, M.; Van Herle, J. Electric vehicle charging station using fuel cell technology: Two different scenarios and thermodynamic analysis. *Energy Rep.* **2021**, *7*, 6955–6972. [CrossRef]
6. Duan, L.; Huang, K.; Pan, X.; Yang, Y. Study on a zero CO_2 emission SOFC hybrid power system integrated with OTM using CO_2 as sweep gas. *Int. J. Energy Res.* **2013**, *37*, 811–824. [CrossRef]
7. Pourrahmani, H.; Matian, M.; Van Herle, J. Poisoning effects of cerium oxide (CeO_2) on the performance of proton exchange membrane fuel cells (PEMFCs). *ChemEngineering* **2022**, *6*, 36. [CrossRef]
8. Pourrahmani, H.; Siavashi, M.; Moghimi, M. Design optimization and thermal management of the PEMFC using artificial neural networks. *Energy* **2019**, *182*, 443–459. [CrossRef]
9. Khalili, M.; Bahnamiri, F.K.; Mehrpooya, M. An integrated process conFigureuration of solid oxide fuel/electrolyzer cells (SOFC-SOEC) and solar organic Rankine cycle (ORC) for cogeneration applications. *Int. J. Energy Res.* **2021**, *45*, 11018–11040. [CrossRef]
10. Andersson, M.; Paradis, H.; Yuan, J.; Sundén, B. Review of catalyst materials and catalytic steam reforming reactions in SOFC anodes. *Int. J. Energy Res.* **2011**, *35*, 1340–1350. [CrossRef]
11. Ghahderijani, M.M.; Barakati, S.M.; Jamshidi, A. Application of stochastic simulation method in reliability assessment of a PV-wind-diesel-SOFC hybrid microgrid. *Int. J. Eng. Technol.* **2012**, *4*, 586. [CrossRef]
12. Taheri, M.H.; Khani, L.; Mohammadpourfard, M.; Aminfar, H.; Akkurt, G.G. Multi-objective optimization of a novel supercritical CO2 cycle-based combined cycle for solar power tower plants integrated with SOFC and LNG cold energy and regasification. *Int. J. Energy Res.* **2022**, *46*, 12082–12107. [CrossRef]
13. Ghazvini, M.; Sadeghzadeh, M.; Ahmadi, M.H.; Moosavi, S.; Pourfayaz, F. Geothermal energy use in hydrogen production: A review. *Int. J. Energy Res.* **2019**, *43*, 7823–7851. [CrossRef]
14. Bakalis, D.P.; Stamatis, A.G. Improving hybrid SOFC-GT systems performance through turbomachinery design. *Int. J. Energy Res.* **2014**, *38*, 1975–1986. [CrossRef]

15. Selvam, K.; Rokni, M.M.; Komatsu, Y.; Sciazko, A.; Kaneko, S.; Shikazono, N. Design point analyses of solid oxide fuel cell-steam cycle combined system: Effects of fuel reforming and bottoming cycle steam parameters. *Int. J. Energy Res.* **2022**, *46*, 10844–10863. [CrossRef]
16. Koyama, M.; Kraines, S.; Tanaka, K.; Wallace, D.; Yamada, K.; Komiyama, H. Integrated model framework for the evaluation of an SOFC/GT system as a centralized power source. *Int. J. Energy Res.* **2004**, *28*, 13–30. [CrossRef]
17. Wang, Z.; Zhang, X.; Rezazadeh, A. Hydrogen fuel and electricity generation from a new hybrid energy system based on wind and solar energies and alkaline fuel cell. *Energy Rep.* **2021**, *7*, 2594–2604. [CrossRef]
18. Tocci, L.; Pal, T.; Pesmazoglou, I.; Franchetti, B. Small scale Organic Rankine Cycle (ORC): A techno-economic review. *Energies* **2017**, *10*, 413. [CrossRef]
19. Aliahmadi, M.; Moosavi, A.; Sadrhosseini, H. Multi-objective optimization of regenerative ORC system integrated with thermo-electric generators for low-temperature waste heat recovery. *Energy Rep.* **2021**, *7*, 300–313. [CrossRef]
20. Konur, O.; Saatcioglu, O.Y.; Korkmaz, S.A.; Erdogan, A.; Colpan, C.O. Heat exchanger network design of an organic Rankine cycle integrated waste heat recovery system of a marine vessel using pinch point analysis. *Int. J. Energy Res.* **2020**, *44*, 12312–12328. [CrossRef]
21. Dai, X.; Shi, L.; Qian, W. Thermal stability of hexamethyldisiloxane (MM) as a working fluid for organic Rankine cycle. *Int. J. Energy Res.* **2019**, *43*, 896–904. [CrossRef]
22. Malico, I.; Carvalhinho, A.P.; Tenreiro, J. Design of a trigeneration system using a high-temperature fuel cell. *Int. J. Energy Res.* **2009**, *33*, 144–151. [CrossRef]
23. Kyriaki, E.; Konstantinidou, C.; Giama, E.; Papadopoulos, A.M. Life cycle analysis (LCA) and life cycle cost analysis (LCCA) of phase change materials (PCM) for thermal applications: A review. *Int. J. Energy Res.* **2018**, *42*, 3068–3077. [CrossRef]
24. Rillo, E.; Gandiglio, M.; Lanzini, A.; Bobba, S.; Santarelli, M.; Blengini, G.A. Life Cycle Assessment (LCA) of biogas-fed Solid Oxide Fuel Cell (SOFC) plant. *Energy* **2017**, *126*, 585–602. [CrossRef]
25. Pourrahmani, H.; Bernier, C.M.I.; Van Herle, J. The application of fuel-cell and battery technologies in unmanned aerial vehicles (UAVs): A dynamic study. *Batteries* **2022**, *8*, 73. [CrossRef]
26. de Oliveira-Assis, L.; Soares-Ramos, E.P.; Sarrias-Mena, R.; García-Triviño, P.; González-Rivera, E.; Sánchez-Sainz, H.; Llorens-Iborra, F.; Fernández-Ramírez, L.M. Simplified model of battery energy-stored quasi-Z-source inverter-based photovoltaic power plant with Twofold energy management system. *Energy* **2022**, *244*, 122563. [CrossRef]
27. Wu, X.-J.; Huang, Q.; Zhu, X.-J. Dynamic modeling of a SOFC/MGT hybrid power system based on modified OIF Elman neural network. *Int. J. Energy Res.* **2012**, *36*, 87–95. [CrossRef]
28. Chitgar, N.; Emadi, M.A.; Chitsaz, A.; Rosen, M.A. Investigation of a novel multigeneration system driven by a SOFC for electricity and fresh water production. *Energy Convers. Manag.* **2019**, *196*, 296–310. [CrossRef]
29. Lemmon, E.W.; Huber, M.L.; Mclinden, M.O. NIST Standard Reference Database 23: Reference Fluid Thermodynamic and Transport Properties-REFPROP, Version 8.0. 2007. Available online: https://www.nist.gov/publications/nist-standard-reference-database-23-reference-fluid-thermodynamic-and-transport-0?pub_id=50520 (accessed on 2 April 2007).
30. Abbasi, H.R.; Pourrahmani, H.; Chitgar, N.; Van herle, J. Thermodynamic analysis of a tri-generation system using SOFC and HDH desalination unit. *Int. J. Hydrogen Energy* **2021**, *in press*. [CrossRef]
31. Gilleran, M.; Bonnema, E.; Woods, J.; Mishra, P.; Doebber, I.; Hunter, C.; Mitchell, M.; Mann, M. Impact of electric vehicle charging on the power demand of retail buildings. *Adv. Appl. Energy* **2021**, *4*, 100062. [CrossRef]
32. *ISO 14040:2006*; Environmental Management—Life Cycle Assessment—Principles and Framework. ISO: Geneva, Switzerland, 2006.
33. *ISO 14044:2006*; Environmental Management—Life Cycle Assessment—Principles and Framework. ISO: Geneva, Switzerland, 2006.
34. Dekker, E.; Zijp, M.C.; van de Kamp, M.E.; Temme, E.H.; van Zelm, R. A taste of the new ReCiPe for life cycle assessment: Consequences of the updated impact assessment method on food product LCAs. *Int. J. Life Cycle Assess.* **2020**, *25*, 2315–2324. [CrossRef]
35. Wernet, G.; Bauer, C.; Steubing, B.; Reinhard, J.; Moreno-Ruiz, E.; Weidema, B. The ecoinvent database version 3 (part I): Overview and methodology. *Int. J. Life Cycle Assess.* **2016**, *21*, 1218–1230. [CrossRef]
36. Ding, Y.; Liu, C.; Zhang, C.; Xu, X.; Li, Q.; Mao, L. Exergoenvironmental model of organic Rankine cycle system including the manufacture and leakage of working fluid. *Energy* **2018**, *145*, 52–64. [CrossRef]
37. Strazza, C.; DEL Borghi, A.; Costamagna, P.; Traverso, A.; Santin, M. Comparative LCA of methanol-fuelled SOFCs as auxiliary power systems on-board ships. *Appl. Energy* **2010**, *87*, 1670–1678. [CrossRef]
38. Marques, P.; Garcia, R.; Kulay, L.; Freire, F. Comparative life cycle assessment of lithium-ion batteries for electric vehicles addressing capacity fade. *J. Clean. Prod.* **2019**, *229*, 787–794. [CrossRef]